J|A|C|S
ARTICLES
Published on Web 10/04/2006

Fabrication of Steady Junctions Consisting of α,ω-Bis(thioacetate) Oligo(*p*-phenylene vinylene)s in Nanogap Electrodes

Tien-Tzu Liang,[†,‡,§] Yasuhisa Naitoh,*[,†,‡] Masayo Horikawa,[†,‡] Takao Ishida,[†,‡] and Wataru Mizutani[†]

Contribution from the Nanotechnology Research Institute, National Institute of Advanced Industrial Science and Technology, 1-1-1 Higashi, Tsukuba, Ibaraki 305-8562, Japan, and Synthetic Nano-Function Materials Project, National Institute of Advanced Industrial Science and Technology, 1-1-1 Umezono, Tsukuba, Ibaraki 305-8568, Japan

Received April 12, 2006; E-mail: ys-naitou@aist.go.jp

Abstract: For obtaining molecular devices using metal−molecule−metal junctions, it is necessary to fabricate a steady conductive bridge-structure; that is stable chemical bonds need to be established from a single conductive molecule to two facing electrodes. In the present paper, we show that the steadiness of a conductive bridge-structure depends on the molecular structure of the bridge molecule for nanogap junctions using three types of modified oligo(phenylene vinylene)s (OPVs): α,ω-bis(thioacetate) oligo(phenylene vinylene) (OPV1), α,ω-bis(methylthioacetate) oligo(phenylene vinylene) (OPV2), and OPV2 consisting of ethoxy side chains (OPV3). We examined the change in resistance between the molecule-bridged junction and a bare junction in each of the experimental Au−OPV−Au junctions to confirm whether molecules formed steady bridges. Herein, the outcomes of whether molecules formed steady bridges were defined in terms of three types of result; *successful*, *possible* and *failure*. We define the ratio of the number of *successful* junctions to the total number of experimental junctions as *successful* rate. A 60% *successful* rate for OPV3 was higher than for the other two molecules whose *successful* rates were estimated to be ∼10%. We propose that conjugated molecules consisting of methylthioacetate termini and short alkoxy side chains are well suited for fabricating a steady conductive bridge-structure between two facing electrodes.

Introduction

For the realization of molecular devices with metal−molecule−metal junctions containing functional molecules, a number of studies have been conducted previous to this study.[1−4] In particular, studies on potential ''molecular nanowires" based on dithiol terminated π-conjugated oligomers is proceeding at a rapid pace. Typical Au−nanowire−Au junctions formed with oligo(phenylene vinylene) (OPV),[5−11] oligo(phenylene ethynylene) (OPE),[5−9,12−17] oligo(phenylene) (OP),[18,19] and oligo(thiophene) (OT),[20−22] have been reported. Since the OPV backbone consists of a higher degree of planarity, and thus better π-conjugation, than those for OPE or the other molecules,[9,23−24] Au−OPV−Au junctions always show higher electronic conductance than other conjugated oligomers.[5−9] For example, Blum et al. showed that the resistance of a cross-wire tunneling

† Nanotechnology Research Institute.
‡ Synthetic Nano-Function Materials Project.
§ Present address: Yokohama Oil & Fats Industry Co., Ltd., 1-1, Minamisenngenncho, Nishiku, Yokohama, 220-0074, Japan.

(1) Aviram, A.; Ratner, M. A. *Chem. Phys. Lett.* **1974**, *29*, 277.
(2) Joachim, C.; Gimzewski, J. K.; Aviram, A. *Nature* **2000**, *408*, 541.
(3) Nitzan, A.; Ratner, M. A. *Science* **2003**, *300*, 1384.
(4) Salomon, A.; Cahen, D.; Lindsay, S.; Tomfohr, J.; Engelkes, V. B.; Frisbie, C. D. *Adv. Mater.* **2003**, *15*, 1881.
(5) Long, D. P.; Patterson, C. H.; Moore, M. H.; Seferos, D. S.; Bazan, G. C.; Kushmerick, J. G. *Appl. Phys. Lett.* **2005**, *86*, 153105.
(6) Blum, A. S.; Kushmerick, J. G.; Pollack, S. K.; Yang, J. C.; Moore, M.; Naciri, J.; Shashidhar, R.; Ratna, B. R. *J. Phys. Chem. B* **2004**, *108*, 18124.
(7) Cai, L. T.; Skulason, H.; Kushmerick, J. G.; Pollack, S. K.; Naciri, J.; Shashidhar, R.; Allara, D. L.; Mallouk, T. E.; Mayer, T. S. *J. Phys. Chem. B* **2004**, *108*, 2827.
(8) Blum, A. S.; Yang, J. C.; Shashidhar, R.; Ratna, B. R. *Appl. Phys. Lett.* **2003**, *82*, 3322.
(9) Kushmerick, J. G.; Holt, D. B.; Pollack, S. K.; Ratner, M. A.; Yang, J. C.; Schull, T. L.; Naciri, J.; Moore, M. H.; Shashidhar, R. *J. Am. Chem. Soc.* **2002**, *124*, 10654.
(10) Naitoh, Y.; Liang, T.-T.; Azehara, H.; Mizutani, W. *Jpn. J. Appl. Phys.* **2005**, *44*, L472.
(11) Azehara, H.; Liang, T.-T.; Ishida, T.; Naitoh, Y.; Mizutani, W. *Jpn. J. Appl. Phys.* **2004**, *43*, 4511
(12) Blum, A. S.; Kushmerick, J. G.; Long, D. P.; Patterson, C. H.; Yang, J. C.; Henderson, J. C.; Yao, Y.; Tour, J. M.; Shashidhar, R.; Ratna, B. R. *Nat. Mat.* **2005**, *4*, 167.
(13) Selzer, Y.; Cabassi, M. A.; Mayer, T. S.; Allara, D. L. *J. Am. Chem. Soc.* **2004**, *126*, 4052.
(14) Reichert, J.; Weber, H. B.; Mayor, M.; Löhneysen, H. v. *Appl. Phys. Lett.* **2003**, *82*, 4137.
(15) Kushmerick, J. G.; Holt, D. B.; Yang, J. C.; Naciri, J.; Moore, M. H.; Shashidhar, R. *Phys. Rev. Lett.* **2002**, *89*, 086802.
(16) Reichert, J.; Ochs, R.; Beckmann, D.; Weber, H. B.; Mayor, M.; Löhneysen, H. v. *Phys. Rev. Lett.* **2002**, *88*, 176804.
(17) Amlani, I.; Rawlett, A. M.; Nagahara, L. A.; Tsui, R. K. *Appl. Phys. Lett.* **2002**, *80*, 2761.
(18) Dadosh, T.; Gordin, Y.; Krahne, R.; Khivrich, I.; Mahalu, D.; Frydman, V.; Sperling, J.; Yacoby, A.; Bar-Joseph, I. *Nature* **2005**, *436*, 677.
(19) Samanta, M. P.; Tian, W.; Datta, S.; Henderson, J. I.; Kubiak, C. P. *Phys. Rev. B* **1996**, *53*, R7626.
(20) Zhitenev, N. B.; Erbe, A.; Bao, Z. *Phys. Rev. Lett.* **2004**, *92*, 186805.
(21) Zhitenev, N. B.; Meng, H.; Bao, Z. *Phys. Rev Lett.* **2002**, *88*, 226801.
(22) Kergueris, C.; Bourgoin, J.-P.; Palacin, S.; Esteve, D.; Urbina, C.; Magoga, M.; Joachim, C. *Phys. Rev. B* **1999**, *59*, 12505.
(23) Liang, T.-T.; Azehara, H.; Ishida, T.; Mizutani, W.; Tokumoto, H. *Synth. Met.* **2004**, *140*, 139.
(24) Seferos, D. S.; Banach, D. A.; Alcantar, N. A.; Israelachvili, J. N.; Bazan, G. C. *J. Org. Chem.* **2004**, *69*, 1110.

10.1021/ja062561h CCC: $33.50

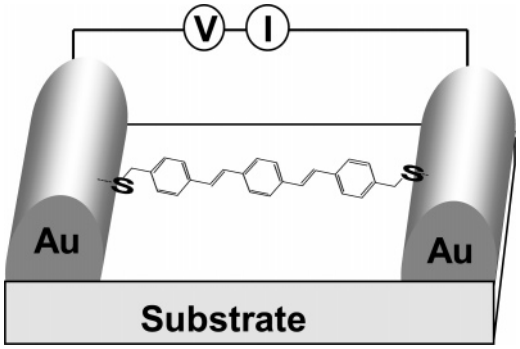

Figure 1. Schematic illustration for *IV* measurements of Au−OPV2−Au junction.

Table 1. Molecular Structures, Spectroscopic Data for the OPV Molecules

Sample	Molecular Structure	Molecular Length [a]	λ_{max} [b] (energy equivalent)	PL [c] (energy equivalent)
OPV1	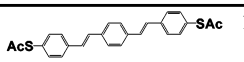	1.97 nm	368 nm (3.37eV)	430 nm (2.88eV)
OPV2	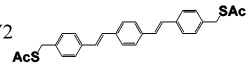	2.12 nm	364 nm (3.41eV)	423 nm (2.93eV)
OPV3	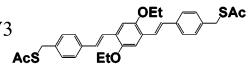	2.10 nm	391 nm (3.17eV)	449 nm (2.76eV)

[a] The calculated length of the molecule from sulfur atom to sulfur atom. [b] Absorption maximum in dichloromethane. [c] Emission maximum in dichloromethane.

junction consisting of self-assembled monolayers (SAMs) of OPV with butoxy side-chain molecules was estimated to be 0.5 ± 0.2 MΩ.[6] They also showed that the cross-wire junction contains ∼1000 molecules as calculated using a resistance of 0.6 ± 0.1 GΩ for single OPV molecules obtained from scanning tunneling microscopy (STM) measurements.[6] We also have successfully measured current−voltage (*IV*) characteristics of Au−polythiophene−Au[25] and Au−OPV−Au junctions[10] (using the setup illustrated in Figure 1) and have confirmed an increase in the conductance of the molecule-bridged junction. In addition, we have measured the dependence of conductance on temperature for the Au−OPV−Au junction yielding characteristic hopping conduction behavior, and the activation energy E_a was estimated to be ∼34 meV.[10]

However, for practical applications of molecular devices, it is very important to fabricate a steady conductive bridge-structure, wherein stable chemical bonds are established from a single conductive molecule to two facing electrodes. We consider that such steadiness of the conductive bridge-structure is dependent on the molecular structure of the bridge molecule, since the possibility of stable chemical bond formation is strongly affected by such a conjugated molecular structure. We have therefore compared the increase in steadiness of a conductive bridge-structure junction using three types of α,ω-bis(thiolate) oligo(phenylene vinylene)s (OPV) molecules as shown in Table 1: 1,4-bis[4′-(thioacetyl)styryl] benzene (OPV1), a fully conjugated molecule; 1,4-bis[4′-(methyl thioacetyl)styryl] benzene (OPV2), in which the conjugation is broken near the Au−S-contacts by a methylene spacer; 1,4-diethoxy-2,5-bis-[4′-(methylthioacetyl)styryl] benzene (OPV3), in which the solubility in organic solvents is improved by introducing ethoxy side chains.

In this paper, the average resistance and activation energy of these three Au−OPV−Au junctions are estimated as reference data for comparing the similar experimental results of other papers.[6,20] The molecular alignment on the Au surface is investigated by X-ray photoelectron spectroscopy (XPS) analysis to discuss the steadiness relationship between bridge-structures.

Experimental Section

The fabrication procedure for sub-5 nm gap electrodes less than 5 nm on a silica chip is described in our previous paper[10] and Supporting Information. The basic experimental processing involves immersing a clean gold surface of sub-5 nm gap electrodes into a solution containing the OPV molecules with thioacetate (−SAc) or methyl thioacetate ($-CH_2SAc$) termini. The protective acetyl groups were removed just prior to immersion of the gold electrodes into the molecule solution. To 4 mL of 0.1 mM OPV2 or OPV3 solution in dichloromethane was added 20 μL of 28% aqueous ammonia, and 1.5 mL of 2 mM pyrrolidine solution in dichloromethane was added to 4 mL of 0.1 mM OPV1 in dichloromethane. The solution was incubated for 10 min to deprotect the thiol group, which converts thioacetate termini to thiolate termini. A clean electrode chip was then immersed into the OPV solution at room temperature for a period of 12−24 h. After removal from the solution, the electrodes were thoroughly rinsed with dichloromethane and then dried with nitrogen. The current through the molecule was measured in a vacuum using an electrometer (Keithley 6517A) for a ±1V bias.

We characterized the monolayer formed from the OPVs on Au surfaces (Au 50 nm/Cr 2 nm evaporated onto silicon oxide/Si), which were fabricated using the same evaporation conditions to fabricate nanogap electrodes, using XPS, sum frequency generation (SFG), ellipsometry, and tapping-mode atomic force microscopy (AFM). The XPS spectroscopy was observed using XPS (Theta Probe-System, Thermo VG Scientific Inc.) with a monochromatic Al Kα X-ray source, 1486.6 eV. The binding energy was calibrated using the Au($4f_{7/2}$) peak energy with 84.0 eV as the energy standard. The X-ray power, the pass energy of the analyzer, and the takeoff angle of photoelectrons were respectively set at 45 W, 50 eV, and 90°. The energy resolution of this system is less than 0.65 eV, as estimated by the Ag($3d_{5/2}$) peak width under our measurement conditions.

Results and Discussions

1. *IV* Characteristics. Initially, we examined the change in *IV* behavior between the bare junction and the molecule-bridged junction for each of the experimental Au−OPV−Au junctions to confirm whether the molecules were steadily bridged. The *IV* behavior changes for the Au−OPV−Au junctions were defined in terms of three types of behavior: *successful*, *possible*, and *failure*. The resistance values of the experimental bare junctions varied from 10 TΩ to 10 MΩ, as calculated from the slopes of the line in the *IV* ohmic region from −0.05 to +0.05 V. Thus, to illustrate the three types of *IV* behaviors, we sorted one set of Au−OPV2−Au junctions in which their bare junctions had a similar resistance, ∼10 GΩ. The *successful*, *possible*, and *failure* exemplifications of the Au−OPV2−Au junction are shown in Figure 2.

In Figure 2(a1) the overall amplitude of the current of the *successful* molecule-bridged Au−OPV2−Au junction is larger than that of its bare junction. In Figure 2(a2), all *IV* curves of the *successful* bridged junction are almost linear lines in the

(25) Naitoh, Y.; Tsukagoshi, K.; Murata, K.; Mizutani, W. *e-J. Surf. Sci. Nanotechnol.* **2003**, *1*, 41.

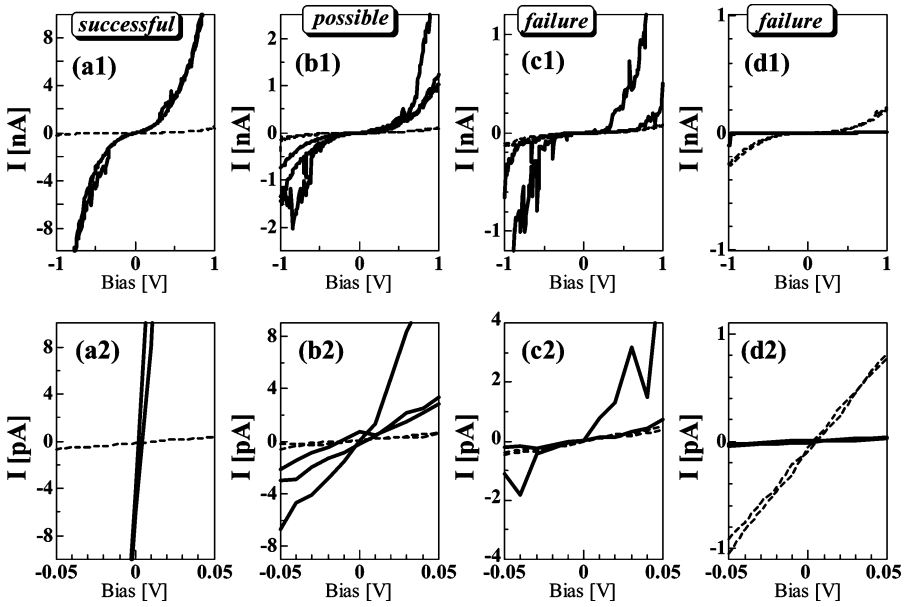

Figure 2. Change in *IV* behavior between a bare junction (dashed line) and the molecule-bridged junction (solid line) shows three types of *IV* behavior for an exemplificative Au−OPV2−Au junction: (a1) *successful*, (b1) *possible*, (c1) and (d1) *failure*. Their *IV* characteristics at ohmic regions are magnified in (a2), (b2), and (c2) and (d2), respectively.

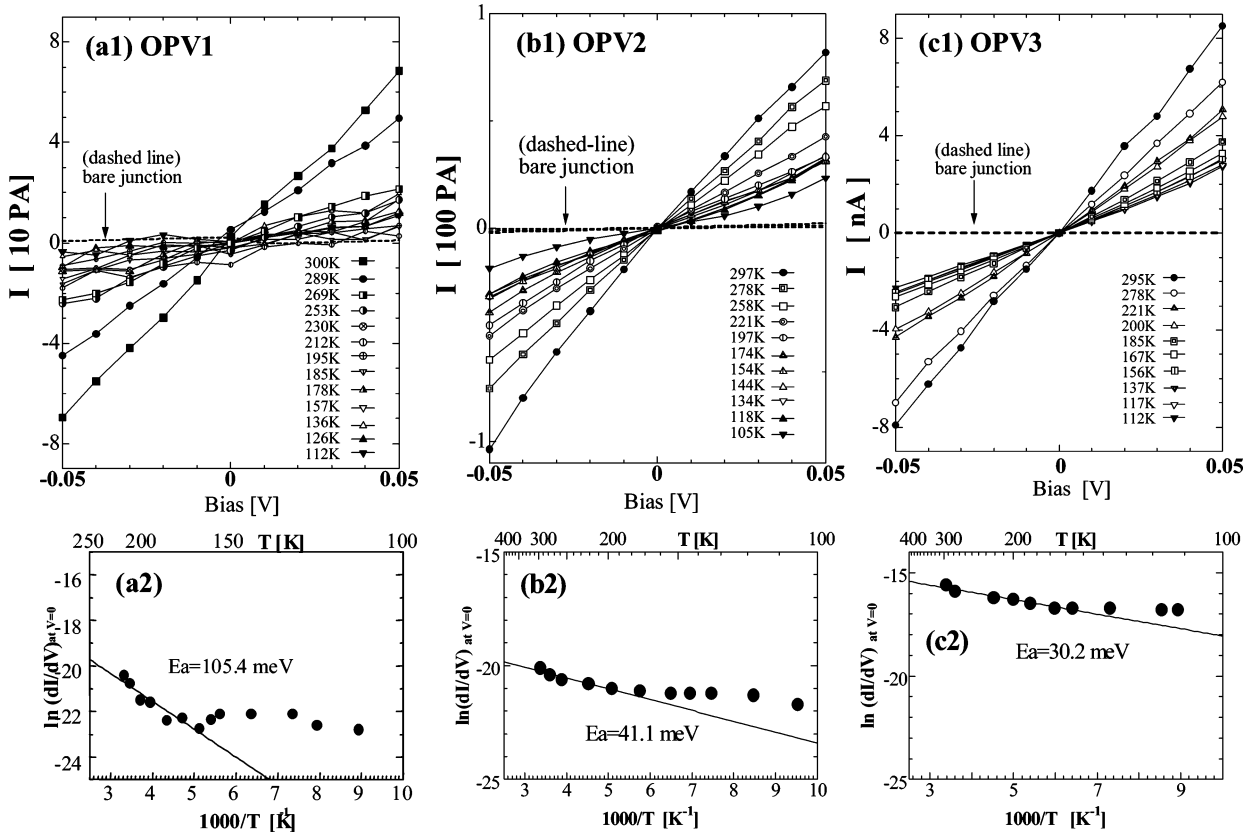

Figure 3. Temperature-dependent *IV* characteristics, the Arrhenius plots of temperature dependence of conductance, and the estimation of E_a for exemplificative *successful* OPV1, OPV2, and OPV3 junctions are shown in (a1,a2), (b1,b2), and (c1,c2), respectively. The estimated activation energies E_a of the OPV1, OPV2, and OPV3 junctions are 66.0, 41.1, 30.2 meV, respectively.

ohmic region, i.e., in the range of −0.05 to +0.05 V. This steady *IV* behavior is interpreted as steady bridge-structure, wherein stable chemical Au−S bonds are formed from a single bridge molecule to two facing electrodes. The temperature-dependent *IV* characteristics of this *successful* Au−OPV2−Au junction at the ohmic region can be clearly observed in Figure 3(b1). Analyzing the data in Figure 3(b1) using the hopping conduction of the equation,[10,13,20]

$$I/V = A_H \exp(-E_a/k_B T) \quad (1)$$

yields Arrhenius plots of the temperature dependence of conductance as shown in Figure 3(b2). A_H is the proportionality constant, and k_B is the Boltzmann constant. The Arrhenius plots

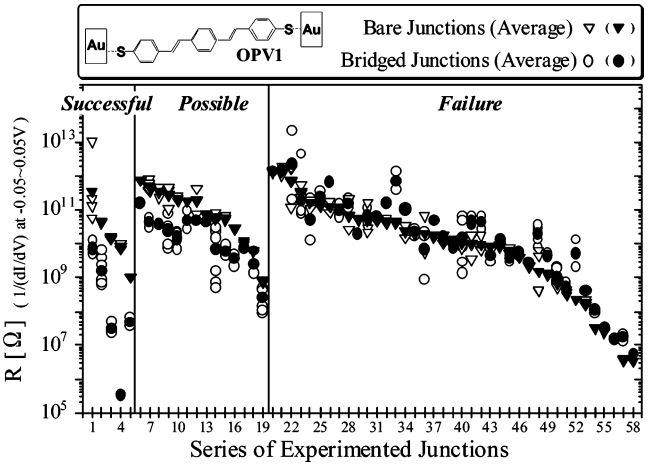

Figure 4. Change in resistance of Au−OPV1−Au junctions between a molecule-bridged junction and a bare junction is defined in terms of three types of results: *successful*, *possible*, and *failure*. The bridging rate is 19/58 (32.8%), and the *successful* rate is 5/58 (8.6%). The resistance R is calculated from the slope of the line in the *IV* ohmic region, from −0.05 to +0.05 V.

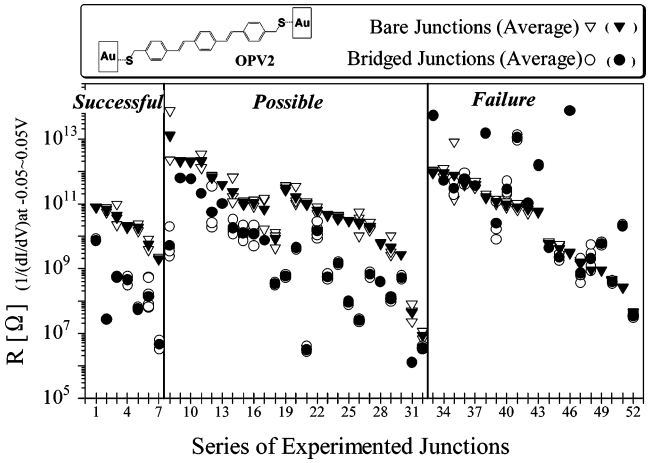

Figure 5. Change in resistance of Au−OPV2−Au junctions between the molecule-bridged junction and the bare junction. The bridging rate is 32/52 (61.5%), and the *successful* rate is 7/52 (13.5%).

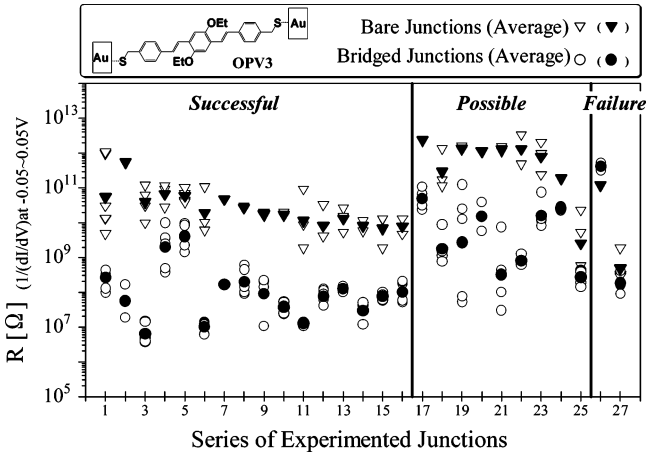

Figure 6. Change in resistance of Au−OPV3−Au junctions between the molecule-bridged junction and the bare junction. The bridging rate is 25/27 (92.6%), and the *successful* rate is 16/27 (59.3%).

show linear dependence around the high-temperature region (≳150 K >) and the activation energy E_a is estimated to be 41.1 meV. Since the temperature dependence in the low-temperature region (≲150 K) was gradually changed, the conduction mechanism is not the simple hopping conduction. However, because we could measure clear temperature dependence in the high-temperature region, it can be considered that the hopping conduction is dominant at least in the region.[13] Similarly, the temperature-dependent *IV* characteristics, the Arrhenius plots, and the estimation of E_a for the exemplificative *successful* Au−OPV1−Au and Au−OPV3−Au junctions are shown in Figure 3(a1,a2) and Figure 3(c1,c2), respectively. The estimated E_a for the OPV1 and OPV3 junctions are 105.4 and 30.2 meV respectively.

In *possible* cases, as shown in Figure 2(b1), the *IV* behavior of the Au−OPV2−Au junction is similar to that of the *successful* junction. However, the currents in these junctions increase unstably in the high-voltage region. Also, a distorted *IV* curve was obtained in the ohmic region as shown in Figure 2(b2). These unstable *IV* behaviors were interpreted as being the result of an unsteady bridge-structure where either of the Au−S bonds of the molecule might be unstable when a higher voltage is applied.

In *failure* cases, as shown in Figure 2(c1) for example, the current amplitude of the molecule-bridged Au−OPV2−Au junction is a slightly higher than that of its bare junction. However, in the ohmic region, the amplitudes of some of the *IV* curves of the *failure* junction are lower than those of its bare junction, as shown in Figure 2(c2). The results indicate that a bridge-structure was not fabricated in the nanogap; i.e., tunneling is the dominant mechanism of the observed current. In Figure 2(d1), another kind of *failure* junction shows that the overall amplitude of the current of the Au−OPV3−Au junction is lower than that of its bare junction. The reverse result was clearly observed in the ohmic region as shown in Figure 2(d2). The reverse behavior was interpreted as due to a brittle bridge-structure; i.e., either of the Au−S bonds of the bridging molecule could separate together with Au atoms from the electrodes, thereby damaging the structure of the electrode.

2. Bridging Rate

The resistance of each of the experimental Au−OPV−Au junctions was calculated from the slope of the line in the *IV* ohmic region, from −0.05 to +0.05 V. The resistances of both the bare junction and the molecule-bridged junction for each of the Au−OPV1−Au junctions are shown in Figure 4. Among the 58 Au−OPV1−Au junction samples examined, there were 19 bridging junctions that contained only 5 *successful* junctions and 14 *possible* junctions. Thus, the bridging rate was 19/58 or 32.8%. After excluding 14 *possible* junctions from the 19 bridging junctions, the *successful* rate was down to 5/58, or 8.6%. In Figure 5, the bridging rate of the Au−OPV2−Au junctions is 32/52 or 61.5%. After excluding 25 *possible* junctions from the 32 bridging junctions, the *successful* rate is only 7/52 or 13.5%. In Figure 6, the bridging rate of the Au−OPV3−Au junction is 25/27 or 92.6%. After excluding 9 *possible* junctions from 25 bridging junctions, the *successful* rate became 16/27 or 59.3%. The bridging-rate trend thus obtained is OPV1 = 32.8% less than OPV2 = 61.5% less than OPV3 = 92.6%. The *successful* rate trend is OPV1 = 8.6% less than OPV2 = 13.5% less than OPV3 = 59.3%. The results indicate that OPV3 is the optimum molecule for the fabrication

Table 2. Elemental Composition Estimated from XPS Peak Areas for OPVs on Au Surfaces

sample	$S(2p_{3/2})$ area ratio of **unbound S** at 163–164 eV	$S(2p_{3/2})$ area ratio of **bound S** at 162 eV	$S(2p_{3/2})$ area ratio of **isolated S** at 161 eV	S(2p)/Au(4f)	C(1s)/Au(4f)
OPV1	33.3%	30.9%	35.6%	0.08	0.74
OPV2	83.1%	16.9%	−	0.14	1.94
OPV3	40.3%	24.2%	35.4%	0.15	0.81

of steady Au−OPV−Au junctions compared to the other OPVs examined in this study.

3. XPS Analysis

We clarify that the increase in the *successful* rate is decided on the basis of the change in molecular alignment morphology resulting from XPS analysis. We have attempted to discuss molecular alignments on the gold surface based on detailed XPS analysis of sulfur peaks, since the peak ratio of the sulfur peak position reflects the molecular alignment and packing density. For XPS measurements, since we only measure chemical states of a molecular layer bound on one side, the detailed surface situation is different from that inside nanogap electrodes. However, we believe that such a measurement is not necessarily meaningless.

It has been reported that the $S(2p_{3/2})$ binding energies for unbound alkane thiols and dialkyl disulfide are between 163 and 164 eV, and after self-assembly of these molecules onto a gold surface, the $S(2p_{3/2})$ binding energy deceases to 162 eV.[26−29] We also found another sulfur species around 161 eV, and this 161 eV peak is often seen in less densely packed SAMs.[28] It was considered that the peak at 161 eV is isolated sulfur, which is assigned to "atomic sulfur produced by C−S cleavage" or "another sulfur without C−S cleavage".[28]

The $S(2p_{3/2})$ peaks of OPV−Au surfaces observed are collected in Table 2 and Figure 7. In the case of OPV1 both the unbound sulfur peak at 163−164 eV and the bound sulfur peak at 162.2 eV were observed. Both the $S(2p_{3/2})$/Au(4f) and C(1s)/Au(4f) ratios of 0.08 and 0.74 for OPV1 were lower than those for OPV2, which were 0.14 and 1.94, respectively. It is considered that in the case of OPV1 a lower surface coverage was formed than that for OPV2. Thus, the molecular axis of OPV1 is tilted onto the gold surface, as shown in Figure 8a, which resulted in low surface coverage. Seferos et al.[24] have also reported that the molecular axis of OPV1 is tilted up to ~30° from the gold surface from ellipsometry measurements, supporting our assumption concerning OPV1. On the other hand, we considered that the molecular axis of OPV2 is vertical to the gold surface as shown in Figure 8b, which resulted in high surface coverage. Thus, the photoelectrons emitted from the bound sulfur atom of OPV2 around 162 eV are partly shielded by the conjugated molecular planes. As shown in Table 2, the $S(2p_{3/2})$ area ratio of bound sulfur is 16.9% for OPV2 and is lower than that of OPV1 at 30.9%.

In addition, the orientation of an aromatic moiety exhibits a pronounced dependence on the length of the alkane spacer, i.e., the number of methylene groups in $R-(CH_2)_m-SH$.[30,31] For m = odd on gold or m = even on silver, the molecules stand up more vertically on the substrates. For m = even on gold or m = odd on silver, the molecular axes tilt onto the metal surface, resulting in low surface coverage. The aligned molecular morphologies of OPV1 and OPV2 on the gold surface as obtained using XPS analysis are also in agreement with this odd−even effect.

In the case of OPV3, as shown in Table 2, the $S(2p_{3/2})$ area ratio of bound sulfur for OPV3. 24.2%, is larger than that of OPV2, 16.9%; i.e., the photoelectrons emitted from the bound sulfur atom of OPV3 which are shielded by the conjugated molecular planes are fewer than those from the bound sulfur atom of OPV2. Thus, the molecular axis of OPV3 is tilted onto the gold surface, as shown in Figure 8c. Likewise, Seferos et al. demonstrated that dithiol-terminated OPV molecules with linear hexyloxy-substituted structures form less ordered SAMs on an Au, surface compared to unsubstituted OPVs, and generally yield low thicknesses.[24]

To follow up on the molecular conformations which were estimated using XPS on Au surfaces, we tried to estimate the thicknesses of the OPV films using the following three methods, sum frequency generation (SFG), ellipsometry, and atomic force microscopy (AFM). In the case of SFG, we can expect to evaluate the molecular angles with focusing on the peaks of phenylenes around 1600 cm^{-1}. However, since the structures of OPVs are symmetrical and the coverage of OPV films is poor, we could not detect clear peaks for all OPVs. In the case of ellipsometry, the measurement of molecular thickness is too sensitive with the light at 60° and 70° angles of incidence. (the analysis of thickness was done using a polyethylene database). Thus, we concluded that it is difficult to determine molecular thickness of a very thin OPV film, even if other researchers could estimate the thickness using this method. Finally, we carried out the comparison of roughness on the Au surface which was measured by AFM. This comparison of roughness was recorded in Table 5 and Supporting Information in the study by Seferos et al.[24] The average roughness was estimated using six root-mean-square values of 2 μm × 2 μm images which were randomly positioned on surfaces. The average roughnesses of bare Au and Au surfaces covered by OPV1, OPV2, and OPV3 films were 0.50, 0.51, 1.03, and 0.56 nm, respectively. The roughness of OPV2 is especially large among four surfaces. The AFM results suggested that the OPV2 film was the thickest and the molecular angle of OPV2 was the closest to vertical among three OPVs as shown in Figure 8. The AFM results were suitable to the thickness which was suggested by the discussion of the shielding effect of sulfur peaks in XPS spectra.

4. Steadiness of Bridge-Structures

We considered that the steadiness of the Au−OPV−Au junctions was dependent on the alignment of OPV molecules on the junction. We propose that after formation of OPV1 steadied alignment, a small number of the as-grown bridged molecules were attracted by neighboring molecules and were then tilted down for agreeing with the lying-down alignment which is illustrated in Figure 8a. By the same token, although

(26) Castner, D. G.; Hinds, K.; Grainger, D. W. *Langmuir* **1996**, *12*, 5083.
(27) Ishida, T.; Hara, M.; Kojima, I.; Tsuneda, S.; Nishida, N.; Sasabe, H.; Knoll, W. *Langmuir* **1998**, *14*, 2092.
(28) Ishida, T.; Choi, N.; Mizutani, W.; Tokumoto, H.; Kojima, I.; Azehara, H.; Hokari, H.; Akiba, U.; Fujihira, M. *Langmuir* **1999**, *15*, 6799.
(29) Ishida, T.; Fukushima, H.; Mizutani, W.; Miyashita, S.; Ogiso, H.; Ozaki, K.; Tokumoto, H. *Langmuir* **2002**, *18*, 83.
(30) Rong, H.-T.; Frey, S.; Yang, Y.-J.; Zharnikov, M.; Buck, M.; Wühn, M.; Wöll, C.; Helmchen, G. *Langmuir* **2001**, *17*, 1582.
(31) Tao, Y.-T.; Wu, C.-C.; Eu, J.-Y.; Lin, W.-L. *Langmuir* **1997**, *13*, 4018.

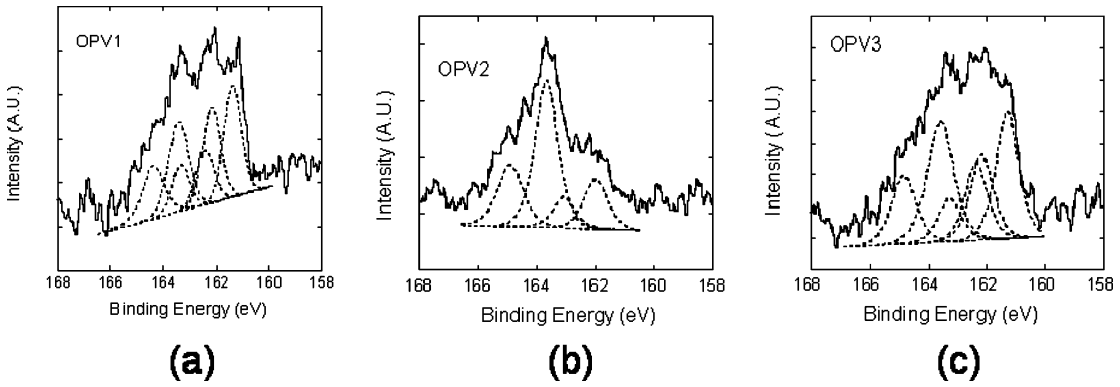

Figure 7. S(2p) XPS spectra of OPV−Au surfaces: (a) OPV1, (b) OPV2, and (c) OPV3.

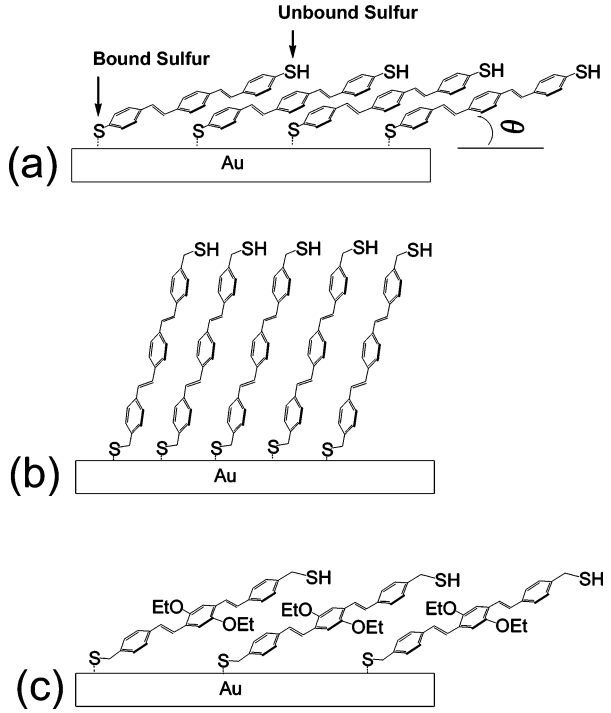

Figure 8. Schematic images of molecular alignments of OPVs on Au surfaces: (a) OPV1, (b) OPV2, and (c) OPV3.

the stand-up alignment of OPV2 might be more likely to form a steady structure than the lying-down alignment of OPV1, the *successful* rate of OPV2 is also poor. We consider that both the molecular angle and the variation of end groups do not necessarily affect to the *successful* rate. However, by comparing the above results of OPV2 and OPV3, it became clear that the presence of the ethoxy parts of OPV molecules work for improvements of the *successful* rate. The reason the ethoxy parts work for the improvements might be explained by the following model. In the bridging using OPV1 or OPV2, the OPVs adsorbed on the gold surface may be tightly fixed by surrounding OPVs, and the orientations of the OPVs are limited. On the other hand, in the case of Au−OPV3−Au junctions, we suggest that the single OPV3 was not so influenced by the neighboring molecules, resulting from the existence of ethoxy side chains. It means that the molecular axis of OPV3 has higher orientational freedom than those of OPV1 and OPV2. The *successful* rate of Au−OPV−Au junctions reflects the dependence on steadiness of the bridge-structures.

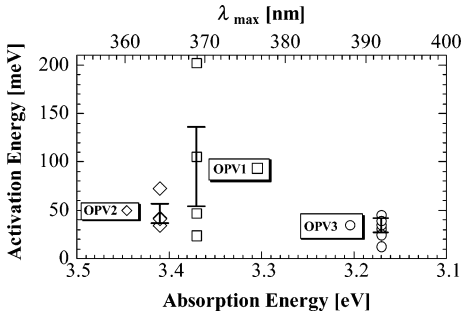

Figure 9. Plot of activation energy of Au−OPV−Au junctions vs absorption energy of the OPV molecules.

5. Conductivity and Activation Energy (E_a)

The estimated resistance trend of the Au−OPV−Au junctions is OPV2 153 ± 91 MΩ > OPV3 92 ± 32 MΩ > OPV1 91 ± 75 MΩ. Although all data show substantial margins of error, we attempted to estimate the number of molecules within an Au−OPV3−Au junction by using the resistance of a single OPV3-like molecule (ethoxy side chains of OPV3 were substituted by butoxy side chains) of 0.6 ± 0.1 GΩ.[6]

At this moment, it is difficult to identify the title angle of the bridged OPV3 molecules as shown in Figure 8c, which changes the conductance of Au−OPV3−Au junctions. However, the number of molecules bridged in an Au−OPV3−Au junction is estimated to be about 10, which is quite small compared to the 1000 molecules of a cross-junction with SAMs of OPV3-like molecules.[6]

The activation energy E_a of hopping conduction for each *successful* Au−OPV−Au junction was also estimated. The average activation energy trend obtained is OPV1 94.5 ± 39.9 meV > OPV2 47.3 ± 8.6 meV > OPV3 33.7 ± 4.3 meV. The estimated activation energies of the OPV junctions match that of dithiol-terminated terthiophene of 10−100 meV.[20]

In addition, we tried to prove a bold assumption that the change of the activation energy of successful Au−OPV−Au junctions depended on the change of the band gap of OPV molecules. Herein, Brédas and Heeger indicated that the band gap of molecules was usually in agreement with the value deduced from optical absorption measurements.[32] The absorption energy trend of the OPV molecules is OPV2 3.41 eV > OPV1 3.37 eV > OPV3 3.17 eV as listed in Table 1. A plot of activation energies of Au−OPV−Au junctions versus absorption energies of OPV molecules is shown in Figure 9. Regrettably,

(32) Brédas, J. L.; Heeger, A. J. *Chem. Phys. Lett.* **1994**, *217*, 507.

an explainable and reliable dependence is not demonstrated in Figure 9 although the three kinds of OPV molecules have the same backbone of 1,4-distyrylbenzene. However, it is clear that the OPV3 molecule of the lowest absorption energy achieved successful Au−OPV3−Au junctions of the lowest activation energy. Especially, the difference in E_a between Au−OPV2−Au and Au−OPV3−Au junctions reveals the effect of side chains, wherein the donor, ethoxy side chains of OPV3, increases the energy level of the HOMO with a reduction in the band gap.[32] It can be considered that the change of the energy level effects the decrease of E_a.

Conclusions

We have demonstrated that the steadiness of a conductive bridge-structure depends on the molecular structure of the bridge molecule. The *successful* rate trend of the Au−OPV−Au junctions is OPV1 8.6% < OPV2 13.5% < OPV3 59.3%, which is commensurate with the shift in steadiness of the conductive bridge-structure: stable chemical bonds are established or broken for a single conductive molecule from two facing electrodes. The elevated *successful* rate of Au−OPV3−Au junctions results from the isolation of the bridged molecular wire between two facing Au surfaces. On the other hand, the OPV1 and OPV2 molecular axes are fixed by the surrounding molecules on the surfaces of electrodes, forming a brittle bridge-structure. We propose that conjugated molecules consisting of methylthioacetate termini and short alkoxy side chains are well suited for fabricating a steady conductive bridge-structure between two facing electrodes.

Acknowledgment. This work was supported by the New Energy and Industrial Development Organization (NEDO) of Japan under the Synthetic Nano-Function Materials Project. We gratefully acknowledge Dr. Hideo Tokuhisa, Dr. Emiko Koyama, and Dr. Yoshinobu Nagawa for their kind support for HPLC purification and NMR identification in the synthesis of OPV, and the measurement of UV-visible spectra. We also gratefully acknowledge Dr. Tohru Nakamura, Dr. Toshitaka Kubo, Dr. Miki Nakano, and Dr. Takayuki Miyamae for their kind support for SFG, ellipsometry, and AFM observation and helpful advice about the molecular angles on Au surfaces.

Supporting Information Available: Synthesis of three types of α,ω-bis(thiolate) oligo(phenylene vinylene) (OPV) molecules; fabrication procedure and SEM images of nanogap electrodes; the Arrhenius plots of temperature dependence of conductance and the estimation of activation energy, E_a, for Au−OPV−Au junctions. This material is available free of charge via the Internet at http://pubs.acs.org.

JA062561H